Communications in Science and Technology 10(2) (2025) 477-492

COMMUNICATIONS IN SCIENCE AND TECHNOLOGY
Homepage: cst.kipmi.or.id

A high-capacity reversible watermarking technique using bit-level expansion and pixel shifting

Aulia Arham, Syukron Abu Ishaq Alfarozi, Hanung Adi Nugroho*

Department of Electrical and Information Engineering, Universitas Gadjah Mada, Yogyakarta 55281, Indonesia

Article history:
Received: 6 December 2025 / Received in revised form: 29 December 2025 / Accepted: 29 December 2025

Abstract

This paper proposes a high-capacity reversible watermarking method using adaptive bit-level expansion and pixel-class-guided shifting. Pixels are classified into expandable (P_0) and non-expandable (P_1) according to their 2-bit LSB patterns, and a lightweight reversible transformation converts P_1 into P_0 with minimal distortion. A shifting map enables exact recovery and avoids overflow/underflow. Secret data are embedded through a 2-bit LSB expansion rule that ensures full reversibility. Experiments on common and medical images demonstrate a consistent embedding capacity of 1.0 bpp, achieving PSNR values above 46 dB and SSIM above 0.97. In addition, the scheme exhibits low computational overhead ($<$0.7s per image, $>$380 kbps) while preserving the original histogram distribution. These results demonstrate that the proposed scheme provides an effective balance between embedding capacity, visual quality, and computational efficiency for secure medical imaging and authenticated reversible data embedding.

Keywords: Reversible watermarking; bit-level expansion; data hiding; pixel-level modification; adaptive embedding.

1. Introduction

Digital watermarking has been widely adopted as a solution for ensuring the security, integrity, and traceability of multimedia content. In sensitive domains such as medical imaging, reversible watermarking is particularly critical as it allows embedded data to be extracted while fully restoring the original image to be fully restored in a lossless manner [1]. This feature is essential for diagnostic accuracy and legal compliance in health information systems, where even minor distortions can affect clinical interpretations.

Among various reversible watermarking approaches, the Difference Expansion (DE) technique has gained significant attention due to its simplicity and high reversibility. Tian's original DE method expanded the difference between pixel pairs to embed data and enables perfect reconstruction of the original image [2]. Several extensions have been introduced to enhance embedding capacity and reduce distortion, such as including histogram shifting, prediction-error expansion, and modulus-based enhancement [3]-[7].

Despite these improvements, existing DE-based methods typically involve trade-offs among embedding capacity, visual quality, computational efficiency, complexity, and the use of an embedding map. In particular, the embedding capacity is limited by the number of pixel pairs satisfying specific embedding conditions, especially in smooth or uniform regions of the image [5]. Furthermore, some pixel values permit expansion of only a single bit (0 or 1), while others may be completely non-expandable. Another constraint is the large size of the embedding map; in many cases, this overhead often exceeds the effective payload. These limitations lead to suboptimal utilization of the available embedding space. From a conceptual perspective, these methods are primarily based on selecting expandable pixels or pixel pairs based on predefined conditions, which prevents them from fully exploiting the theoretical embedding capacity.

To overcome this limitation, this paper introduces an alternative view on pixel expandability. Instead of passively selecting only expandable pixels, we systematically transform non-expandable and partially expandable pixel values into expandable pixel values through controlled bit-level normalization. Based on this perspective, we propose a high-capacity reversible watermarking technique that leverages a bit-level expansion mechanism based on the 2-bit least significant bits (LSB) of each pixel. An adaptive pixel modification strategy minimally adjusts pixel values to make all pixels eligible for embedding, thereby reformulating the expandability constraint

*Corresponding Author.
Email: adinugroho@ugm.ac.id
https://doi.org/10.21924/cst.10.2.2025.1856

from a selection problem into a value-adjustment problem. This transformation is recorded using a shifting map to ensure reversibility and accurate data recovery. The proposed technique is designed to maintain low distortion while approaching the theoretical payload limit of 1 bpp under reversible constraints.

The major contributions of this paper are summarized as follows:

- A novel reversible watermarking framework that casts pixel expandability constraints into a bit-level normalization framework, enabling higher effective payload utilization.
- We introduce a reversible watermarking scheme that employs bit-level expansion using the 2-bit least significant bits (LSB) of each pixel, resulting in compact embedding and reduced distortion.
- An adaptive pixel-shifting method is developed to convert non-expandable or partially expandable pixels into fully expandable pixels while preserving reversibility.
- A compact shifting map design is proposed to record pixel modifications with low overhead, ensuring lossless image reconstruction and accurate data extraction.
- Comprehensive experiments are conducted on both common and medical image datasets, demonstrating improved performance of the proposed method in terms of capacity, visual quality, and embedding capacity compared to several state-of-the-art techniques.

The remainder of the paper is organized as follows: Section II provides a review of related work and the state of the art. Section III describes the proposed method, including the adaptive pixel shifting, data embedding, and extraction procedures. Section IV presents the experimental results and comparative performance analysis. Section V concludes the paper with a summary of findings and directions for future research.

2. State of the Art

Reversible Data Hiding (RDH) is a data embedding technique that permits lossless restoration of the original image after the embedded data has been extracted. Over the past two decades, numerous RDH approaches have been developed to address key challenges in RDH, with an emphasis on balancing embedding capacity, visual fidelity, and computational efficiency. These techniques can be broadly categorized into four major groups: (1) Difference Expansion (DE)-based methods, (2) Histogram Modification (HM)-based methods, (3) Prediction-Error Expansion (PEE)-based methods and differencing-based methods, and (4) RDH in Encrypted Images (RDHEI).

2.1. Difference Expansion and Its Variants

Difference Expansion (DE) was first introduced by Tian [2], where data are embedded by expanding the difference values between neighboring pixel pairs. This approach achieves a good trade-off between embedding capacity and visual imperceptibility, making it suitable for many practical scenarios. However, classical DE methods often suffer from pixel overflow/underflow, limited embedding capacity, and visual degradation in complex or textured regions.

In response to these limitations, researchers have developed several enhancements to DE. A notable line of research is the use of block-based DE, where data embedding is performed over small pixel blocks rather than individual pairs. For instance, Arham et al. [8] and Al Huti et al. [9] implemented DE within 2×2 and 4×4 blocks, respectively, achieving better localization of modifications and smoother distortion distribution. In a related study, [10] proposed a modified reversible DE (RDE) using 2×2 blocks to minimize pixel differences, thereby enhancing overall embedding performance.

Another line of research utilizes image characteristics for selective and adaptive embedding. For example, visually smooth regions, which are more visually sensitive, are selected for embedding in [11], thereby minimizing perceptual impact. Moreover, DE has been combined with modular arithmetic in [4] to extend embedding flexibility and maintain reversibility.

To further refine DE-based embedding structures, various authors have explored alternative embedding structures. For example, [3] used a 1×3 pixel block design to preserve image quality, at the expense of reduced payload. Meanwhile, [5] significantly improved the method in [4] by embedding 3 bits into 2-bit LSB differences of pixel pairs within 2×2 quad blocks using a difference range of [-2, 1], thereby achieving higher capacity and good visual quality.

In parallel, other DE variants have been integrated into hybrid embedding frameworks. A notable example is [12], which combines linear and quadratic DE for different payload portions and merges processed and unprocessed pixels to generate the final marked image, resulting in improved visual quality and full reversibility. Another enhancement comes from [13], which introduces reduced DE within block-based structures and encrypted payload bits, maintaining fidelity while increasing payload.

Despite these innovations, most DE-based techniques still suffer from limited pixel embeddability, meaning only a subset of pixel values can be used for embedding, and some methods require auxiliary location maps or side information to guide extraction and recovery. This leads to inefficiencies in both embedding and restoration processes, especially in scenarios where high capacity and low distortion are both critical applications such as medical imaging.

2.2. Histogram Modification and Expansion Bin Selection

Histogram-based RDH techniques primarily focus on altering the statistical distribution of pixel values or prediction errors to create embedding space. The use of multiple histogram pairs, as in the Multiple Histogram Modification (MHM) method [14, 15], has demonstrated favorable capacity–distortion trade-offs by utilizing expansion bins optimized according to histogram peak sharpness.

Subsequent developments such as Adaptive MHM [16] integrate pixel correlation and error shiftability to dynamically construct histogram sequences for embedding, enabling better exploitation of local redundancy. Further optimization of expansion-bin selection has enhanced embedding performance and adaptability. Furthermore, the general expansion-shifting

framework proposed in [17] formulates reversible embedding as a constrained optimization problem and derives near-optimal solutions that minimize distortion using Reversible Embedding Functions (REFs). However, these approaches primarily rely on global histogram properties and can be less effective in complex textured images where fine-grained local adaptation is required.

2.3. Prediction-Error Expansion and Content-Adaptive Methods

Prediction-Error Expansion (PEE) methods enhance embedding efficiency through local spatial correlation. Approaches such as enhanced pairwise PEE [18], dual pairwise PEE [19], and adaptive PEE (APPEE) [20] propose improved prediction models and mapping strategies to enhance embedding efficiency and reduce visual distortion.

Another spatial domain technique presented in [21] enhances smooth regions by rearranging image columns or rows prior to data embedding. The approach involves generating an index map and applying histogram shifting on difference matrices to embed data. This rearrangement not only improves the smoothness of regions, enabling more efficient embedding but also achieves a capacity increase of more than 50% while maintaining high visual quality. Moreover, the method is shown to be undetectable under pixel difference histogram (PDH) analysis, thereby enhancing the security of the hidden data. For textured images, the embedding capacity more than doubles compared to conventional methods, demonstrating the strength of spatial pre-processing in RDH schemes.

More advanced techniques adopt learning-based and statistical predictors, including ridge regression [22] and spatially aware prediction models [23]. These models improve accuracy in error estimation, resulting in reduced distortion after embedding. Additionally, the study in [24] explores the theoretical optimization limits of prediction-error-based watermarking, demonstrating that the associated optimization problems are NP-hard and proposing integer linear programming to derive optimal bounds.

Another direction in content-adaptive embedding is the use of pixel-value differencing (PVD) methods. The approach in [25] proposes a dual-image-based RDH scheme, where secret data are embedded based on the maximum pixel difference within non-overlapping blocks. The method calculates the embeddable length using logarithmic scaling and distributes decimal secret data into two stego-images. By leveraging inter-image correlation, the scheme achieves high embedding capacity while maintaining imperceptible distortion. This dual-image PVD strategy proves effective for both smooth and textured cover images.

Additionally, hybrid methods such as PVO-based RDH with self-learning 2D histogram mapping [26] further advance the adaptability of embedding strategies to image content, achieving high PSNR while maintaining embedding performance. Meanwhile, techniques such as interpolated PEE with modulo operation [27] integrate interpolation-based prediction with histogram shifting to maximize capacity while preventing underflow/overflow.

2.4. Reversible Data Hiding in Encrypted Images (RDHEI)

RDHEI techniques enable data embedding in the encrypted domain, thereby ensuring both confidentiality and reversibility. Methods such as local difference predictor embedding [28], intra-block lossless compression [29], and adaptive MSB prediction [30] have demonstrated high payload with low perceptual distortion. Compression-based approaches such as the method in [31], employ blockwise encryption and pixel-difference compression, to further increase payload while maintaining visual quality.

Innovative approaches like recursive bit-plane embedding [32] and hierarchical label mapping [33] have reported embedding capacities exceeding 2.4 bpp and reaching up to 3.6 bpp on certain datasets. Nonetheless, these methods typically involve high computational cost and require synchronized encryption/decryption pipelines.

2.5. Research Gaps and Contribution of This Work

Although many existing RDH techniques achieve a satisfactory balance between embedding capacity and image quality, several issues remain unresolved:

- **Incomplete Pixel Utilization:** Many DE and PEE methods are constrained by limited pixel embeddability leaving a large portion of pixel values unused.
- **Overhead in Embedding Maps:** The need for auxiliary information such as location maps or flags reduces net payload.
- **Computational Complexity:** Prediction and multi-stage optimization increase computational complexity, limiting practicality in large-scale or time-sensitive applications.

To address these challenges, this paper proposes an adaptive reversible watermarking technique based on bit-level expansion using the 2-bit least significant bits (LSB) of each pixel. The method incorporates predefined modification rules and adaptive pixel shifting applied before and after the embedding and extraction process. This approach effectively converts non-expandable pixels into expandable ones through minimal and reversible transformations. The proposed scheme achieves an embedding capacity of up to 1 bpp while preserving visual quality and ensuring computational efficiency, making it particularly suitable for medical image protection and real-time applications.

3. Proposed Method

To address the trade-offs between embedding capacity, image quality, and reversibility in reversible watermarking, this study introduces a novel high-capacity reversible watermarking framework. The method is based on bit-level expansion of the two least significant bits (LSB), combined with an adaptive pixel shifting strategy to convert non-expandable pixels into expandable ones. The overall workflow is illustrated in Fig. 1.

3.1. Bit-Level Expansion Watermarking

Let a grayscale pixel $p \in [0,255]$ be decomposed into:

$$x = p \bmod 4, \qquad y = \left\lfloor \frac{p}{4} \right\rfloor,$$

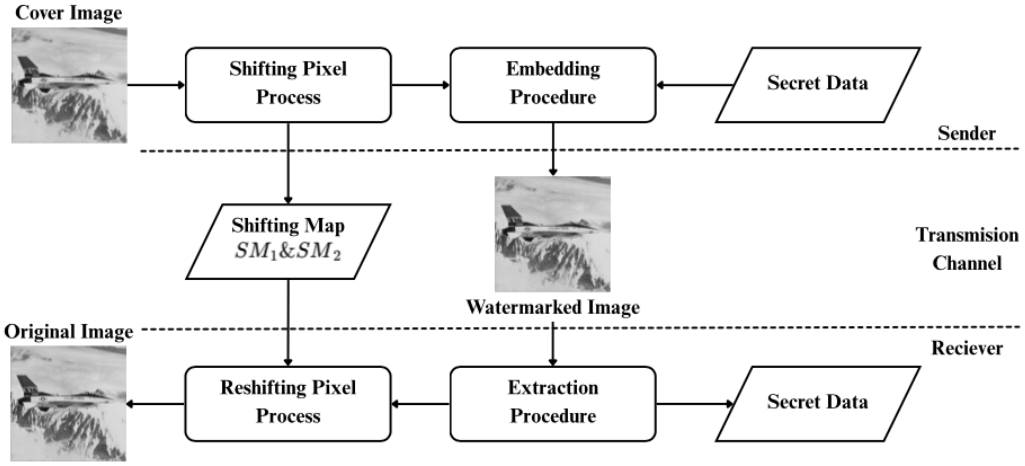

Fig. 1. Block diagram of the proposed method.

where x represents the 2-bit LSB and y contains the remaining 6 MSB.

To embed a secret bit $b \in \{0,1\}$, the proposed method expands the 2-bit LSB using:

$$x' = 2x + b. \tag{1}$$

Because $x \in \{0,1,2,3\}$, the expanded value x' may range from 0 to 7. To preserve reversibility, only the values satisfying:

$$x' \in [0,3] \tag{2}$$

are allowed for embedding. Otherwise, the pixel is considered non-expandable.

When x' is valid, the watermarked pixel is reconstructed as:

$$\tilde{p} = 4y + x'. \tag{3}$$

3.2. Embedding Constraint and Pixel Classification

The embeddability condition must hold for both secret bits $b \in \{0,1\}$. That is,

$$2x + b \leq 3, \quad \forall b \in \{0,1\}. \tag{4}$$

Because $b = 1$ results in the maximum expansion, data embedding is possible only under the following condition:

$$x \in \{0,1\}.$$

Based on this constraint, the pixel domain $[0,255]$ is partitioned into two disjoint sets:

$$P_0 = \{p \mid p \bmod 4 \in \{0,1\}\}, \tag{5}$$
$$P_1 = \{p \mid p \bmod 4 \in \{2,3\}\}. \tag{6}$$

Pixels in P_0 are directly expandable for watermark embedding, while pixels in P_1 are non-expandable and require modification.

3.3. Adaptive Pixel Shifting

To increase the number of expandable pixels, an adaptive pixel shifting mechanism is designed to transform non-expandable pixels from P_1 into the expandable domain P_0. Specifically, each pixel in P_1 is shifted by subtracting 2:

$$p' = p - 2. \tag{7}$$

This is valid because:

$$p \bmod 4 = 2 \Rightarrow (p-2) \bmod 4 = 0,$$
$$p \bmod 4 = 3 \Rightarrow (p-2) \bmod 4 = 1.$$

Thus, all shifted values fall within P_0. Since all pixels in P_1 satisfy $p \geq 2$, the operation never causes underflow.

A one-bit Shifting Map (SM) is recorded to ensure perfect reversibility:

- $SM = 0$ for pixels originally in P_0 (no modification),
- $SM = 1$ for pixels shifted from P_1 to P_0.

Table 1 summarizes the modification rules.

Table 1. Adaptive Shifting Rules and Shifting Map

Original Set	New Set	*SM*	Shift	Undo Shift
P_0	P_0	0	p	p'
P_1	P_0	1	$p-2$	$p'+2$

An illustration of the shifting process is shown in Fig. 2.

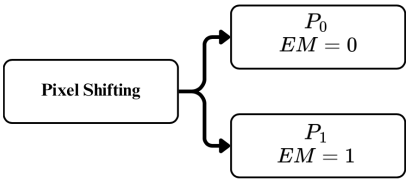

Fig. 2. Shifting process and Shifting Map generation.

3.4. Correctness of Adaptive Shifting

We provide a formal proof that the proposed shifting strategy always maps non-expandable pixels into the expandable domain while ensuring reversibility.

Lemma 1. Transformability

We first recall the definitions of the two pixel sets:

$$P_1 - 2 = P_0.$$

Proof of $P_1 - 2 = P_0$

We begin by recalling the definitions of the two pixel sets:

$$P_0 = \{\, p \mid p \bmod 4 \in \{0,1\}\,\}, \qquad P_1 = \{\, p \mid p \bmod 4 \in \{2,3\}\,\}.$$

Consider any pixel $p \in P_1$. If $p \bmod 4 = 2$, then subtracting 2 yields

$$(p-2) \bmod 4 = 0,$$

a pixel value that belongs to P_0. Likewise, if $p \bmod 4 = 3$, then

$$(p-2) \bmod 4 = 1,$$

which also lies in P_0.

Furthermore, because the smallest pixel value in P_1 is 2, subtracting 2 does not cause underflow, and the resulting pixel value always remains in the valid range $[0,255]$.

Therefore, shifting each $p \in P_1$ by subtracting 2 produces exactly the set P_0, establishing that

$$P_1 - 2 = P_0.$$

Conclusion

The adaptive shifting strategy converts all non-expandable pixels into expandable ones while ensuring full reversibility during extraction using the Shifting Map.

3.5. Embedding Procedure

The embedding process begins with a pre-processing stage in which non-expandable pixels are adaptively shifted to satisfy embeddability constraints. All modifications are recorded in the Shifting Map (SM). Once pre-processing is completed, secret bits are embedded using the proposed bit-level expansion strategy. A detailed description of the proposed embedding procedure is provided in Algorithm 1.

1. For each pixel p' (after shifting), extract:
   - Extract $x = p' \bmod 4, y = \lfloor \frac{p}{4} \rfloor$.
2. Fetch one secret bit $b \in \{0,1\}$.
3. Compute expanded LSB: $x' = 2x + b$.
4. Construct the watermarked pixel: $\tilde{p} = 4y + x'$.

Algorithm 1 Embedding Process

Require: Shifted image p', secret bitstream B
Ensure: Watermarked image $\tilde{p}$
for each pixel p' **do**
  $x = p' \bmod 4$
  $y = \lfloor \frac{p}{4} \rfloor$.
  Get bit b from B
  $x' = 2x + b$
  $\tilde{p} = 4y + x'$
end forreturn $\tilde{p}$

3.6. Extraction Procedure

The extraction process begins by reversing the embedding through bit-level inverse expansion, followed by adaptive pixel reshifting based on the Shifting Map (SM) to restore the original image perfectly. A detailed description of the proposed extraction procedure is provided in Algorithm 2.

1. For each watermarked pixel $\tilde{p}$, extract:
   - $x' = \tilde{p} \bmod 4, y' = \left\lfloor \frac{\tilde{p}}{4} \right\rfloor$.
2. Recover the original 2-bit LSB: $b = x' \bmod 2$.
3. Recover original x: $x = \left\lfloor \frac{x'}{2} \right\rfloor$.
4. Recover the pre-shifted pixel: $p' = 4y' + x$.
5. Apply adaptive reshifting (using SM) to obtain the original pixel p

Algorithm 2 Extraction Process

Require: Watermarked image $\tilde{p}$, Shifting Map SM
Ensure: Extracted bitstream B, recovered original image p
for each pixel $\tilde{p}$ **do**
  $x' = \tilde{p} \bmod 4$
  $y' = y' = \left\lfloor \frac{\tilde{p}}{4} \right\rfloor$
  $b = x' \bmod 2$
  $x = \left\lfloor \frac{x'}{2} \right\rfloor$
  $p' = 4y' + x$
  Apply reshifting according to SM to obtain p
end forreturn B, p

Fig. 3 presents a step-by-step example illustrating the complete embedding and extraction workflow of the proposed method.

4. Experimental Results and Analyses

This section evaluates the proposed method using six grayscale common images and six grayscale medical images, each with a resolution of 512×512 pixels. The images are obtained from the USC-SIPI dataset [34] and medical image libraries [35], as shown in Figs. 4 and 5.

For fair benchmarking, the performance is compared with three existing reversible watermarking methods [4], [3], and [5], all implemented and evaluated using the same datasets, under the same image resolutions and embedding conditions using consistent experimental settings, including capacity-related metrics (embedding capacity C (bits) and capacity per pixel CP (bpp)), computational efficiency (computation time CT (s) and embedding rate ER (bits/s)), and visual quality (PSNR and SSIM). The experiments were performed using MATLAB R2022b running on macOS Monterey (version 12) on a system equipped with an Intel Core i5 processor (2.9 GHz) and 8 GB RAM.

Table 2. Performance Evaluation on Common and Medical Image Sets.

Evaluation	Methods	Common Images						Medical Images					
		Airplane	**Baboon**	**Barbara**	**Boat**	**Tank**	**Peppers**	**Angiogram**	**CT**	**Echocardiogram**	**MRI**	**Radiograph**	**Ultrasonography**
C(bits)	[4]	72,199	20,661	37,138	34,351	37.319	45,844	79,246	78,235	97,246	66,529	96,941	88,700
	[3]	96,315	27,518	49,157	46,017	49,543	60,655	106,251	104,664	129,783	89,134	128,387	117,832
	[5]	100,618	98,253	97,537	96,057	96,544	98,164	147,650	144,229	153,978	114,543	107,583	141,013
	Proposed	262,114	262,114	262,114	262,114	262,114	262,114	262,114	262,114	262,114	262,114	262,114	262,114
CP(bpp)	[4]	0.2754	0.0788	0.1417	0.1310	0.1424	0.1749	0.3023	0.2984	0.3710	0.2538	0.3698	0.3384
	[3]	0.3674	0.1050	0.1875	0.1755	0.1890	0.2314	0.4053	0.3993	0.4951	0.3400	0.4898	0.4495
	[5]	0.3838	0.3748	0.3721	0.3664	0.3683	0.3745	0.5632	0.5502	0.5874	0.4369	0.4104	0.5379
	Proposed	1.0000	1.0000	1.0000	1.0000	1.0000	1.0000	1.0000	1.0000	1.0000	1.0000	1.0000	1.0000
CT(s)	[4]	4.15	4.04	4.55	4.05	4.02	4.03	4.03	4.22	4.16	4.20	4.05	4.07
	[3]	4.58	4.70	4.44	4.41	4.79	4.67	4.44	4.60	4.56	4.59	4.41	4.40
	[5]	4.72	4.76	5.06	4.66	5.17	4.64	4.77	4.74	4.75	4.79	4.66	4.64
	Proposed	0.62	0.61	0.66	0.62	0.62	0.62	0.62	0.62	0.61	0.62	0.62	0.62
ER(bits/s)	[4]	17,414	5,120	8,159	8,482	9,276	11,379	19,649	18,522	23,388	15,829	23,924	21,820
	[3]	21,039	5,857	11,084	10,435	10,345	12,997	23,925	22,743	28,474	19,440	29,093	26,780
	[5]	21,322	20,637	19,268	20,635	18,681	21,147	30,941	30,422	32,437	23,898	23,067	30,424
	Proposed	420,102	426,944	395,390	425,558	421,453	422,812	420,102	424,868	426,944	423,495	425,558	424,181
PSNR (dB)	[4]	50.4705	55.2637	52.8670	53.1846	52.6038	51.9203	54.3954	53.8683	52.9285	51.7830	49.7472	52.2351
	[3]	49.2558	53.9556	51.6900	51.9559	51.3881	50.6922	53.0819	52.6287	51.6856	50.5113	48.5294	51.0283
	[5]	53.6038	53.6223	53.7015	53.7010	53.9745	53.6991	52.9081	52.9166	52.7141	53.3233	53.4927	52.9620
	Proposed	46.3407	46.3652	46.4095	46.5825	46.4652	46.3760	48.0528	47.9388	48.3323	45.9242	46.5814	47.8101
SSIM	[4]	0.9940	0.9992	0.9971	0.9978	0.9983	0.9963	0.9933	0.9931	0.9909	0.9941	0.9912	0.9924
	[3]	0.9923	0.9990	0.9963	0.9972	0.9978	0.9952	0.9893	0.9890	0.9860	0.9917	0.9885	0.9884
	[5]	0.9976	0.9993	0.9985	0.9985	0.9989	0.9980	0.9872	0.9875	0.9850	0.9953	0.9951	0.9881
	Proposed	0.9873	0.9962	0.9919	0.9921	0.9938	0.9888	0.9773	0.9772	0.9721	0.9678	0.9805	0.9765

Note - C(bits): Capacity embedding; CP(bpp): Capacity per pixel; CT(s): Computational time; ER(bits/s): Embedding rate; PSNR(dB): Peak Signal-to-Noise Ratio; SSIM: Structural Similarity Index Measure.

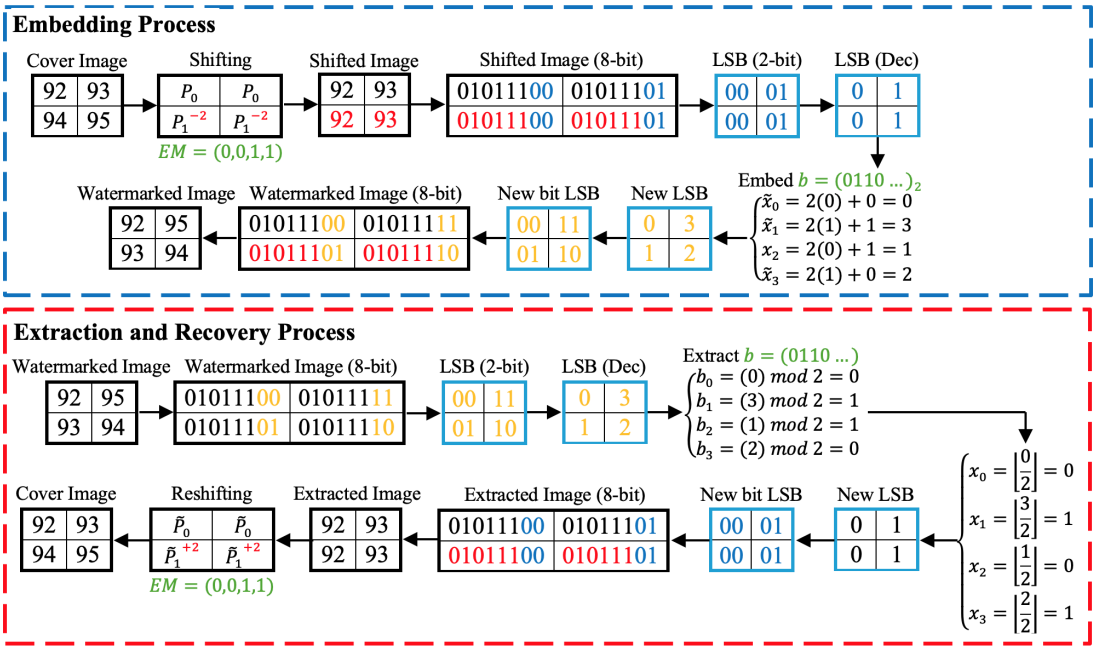

Fig. 3. Illustration of the embedding and extraction processes of the proposed method.

(a) (b) (c) (d) (e) (f)

Fig. 4. Six common images used for testing: (a) Airplane, (b) Baboon, (c) Barbara, (d) Boat, (e) Tank, and (f) Peppers. [34].

4.1. *Embedding Capacity Analysis*

The proposed method achieves a consistent embedding capacity of 262,114 bits (1.0 bpp) across all tested images, outperforming existing approaches. As shown in Table 2 and Fig. 6, previous methods such as [4], [3], and [5] reach capacities ranging from approximately 20,000 to 153,000 bits (0.08–0.59 bpp), depending on the image type. Fig. 6 visually confirms that the proposed adaptive expansion strategy enables near-complete utilization of available pixels, resulting in a stable maximum capacity across different image contents.

It should be noted that achieving the theoretical maximum capacity of 1.0 bpp inherently involves a trade-off between embedding capacity and visual quality, as commonly reported in reversible data hiding literature. In the proposed method, this trade-off is addressed through an adaptive expansion strategy and bit-level pixel classification, which converts non-expandable and partially expandable pixels into expandable pixel values using minimal and reversible modifications. As a result, the consistent 1.0 bpp embedding indicates the stability of the proposed approach across varying image contents while maintaining acceptable visual fidelity.

4.2. *Visual Quality Analysis*

To evaluate the perceptual quality of the watermarked images, we evaluate visual quality using two standard metrics: Peak Signal to-Noise Ratio (PSNR) calculated using Eq. 9 and Structural Similarity Index (SSIM) calculated using Eq. 10. While PSNR quantifies pixel-wise distortion, SSIM captures structural similarity from the perspective of the human visual system.

$$MSE(O, O_W) = \frac{1}{PQ} \sum_{k}^{P-1} \sum_{l}^{Q-1} |O(k,l) - O_W(k,l)|^2 \tag{8}$$

$$PSNR(O, O_W) = 10 \log_{10} \frac{255^2}{MSE} \tag{9}$$

$$\begin{aligned} \mathrm{SSIM}(O, O_W) = {} & [l(O, O_W)]^{\alpha} \cdot [c(O, O_W)]^{\beta} \\ & \cdot [s(O, O_W)]^{\gamma} \end{aligned} \tag{10}$$

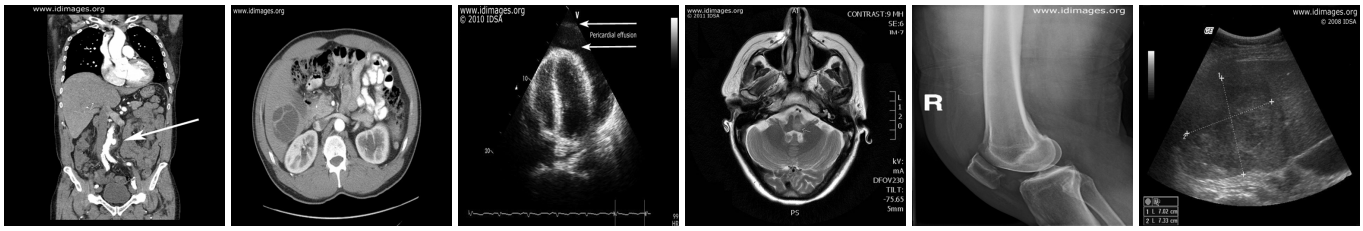

(a) (b) (c) (d) (e) (f)

Fig. 5. Six medical images used for testing: (a) Angiogram, (b) CT (c) Echocardiogram, (d) MRI, (e) Radiograph, and (f) Ultrasonography. [35].

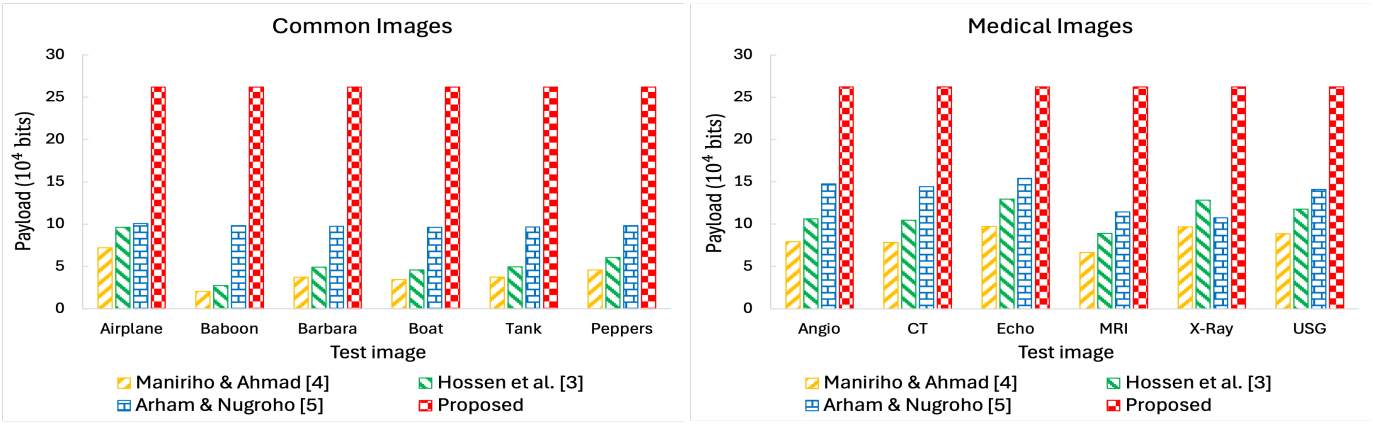

(a) (b)

Fig. 6. Comparison of payload capacity between the proposed method and existing methods for (a) common images and (b) medical images.

where

$$l(O,O_W) = \frac{2\mu_O\mu_{O_W} + C_1}{\mu_O^2 + \mu_{O_W}^2 + C_1} \tag{11}$$

$$c(O,O_W) = \frac{2\sigma_O\sigma_{O_W} + C_2}{\sigma_O^2 + \sigma_{O_W}^2 + C_2} \tag{12}$$

$$s(O,O_W) = \frac{\sigma_{OO_W} + C_3}{\sigma_O\sigma_{O_W} + C_3} \tag{13}$$

The symbols used in Eqs. 10–13 are defined as follows. The terms μ_O and μ_{O_W} denote the mean intensities of the original and watermarked images, respectively. The quantities σ_O and σ_{O_W} represent their standard deviations, while σ_{OO_W} denotes the cross-covariance between the two images. The constants C_1, C_2, and C_3 are stabilization factors defined as $C_1 = (K_1L)^2$, $C_2 = (K_2L)^2$, and $C_3 = C_2/2$, with $L = 255$ for 8-bit images. The exponents α, β, and γ control the relative importance of luminance, contrast, and structure, and are set to 1 following standard practice.

Despite prioritizing high embedding capacity, the proposed method maintains acceptable perceptual quality, particularly on common images. At full embedding capacity (262,114 bits or 1.0 bpp), the PSNR values on common images range from 46.34 dB to 48.33 dB, while SSIM values remain high, between 0.9873 and 0.9962, indicating that visual distortions are mild and structurally non-disruptive. Although the proposed method incurs some loss in visual fidelity due to its significantly higher payload compared with existing techniques, the obtained SSIM levels confirm that the marked images remain visually acceptable.

Compared to existing reversible data hiding schemes by Maniriho & Ahmad [4], Hossen et al. [3], and Arham & Nugroho [5], the proposed method achieves considerably higher embedding capacity but with lower PSNR, as expected in high-capacity scenarios. For instance, on the Airplane image at full embedding, the proposed method yields 46.34 dB, whereas Maniriho & Ahmad [4], Hossen et al. [3], and Arham & Nugroho [5] report 50.47 dB, 49.25 dB, and 53.60 dB respectively. A consistent trend is observed across Baboon, Barbara, Boat, Tank, and Peppers, where competing methods achieve higher PSNR but at much lower payloads (typically below 0.38 bpp), as shown in Table 2.

On medical images, a similar trend appears. The proposed method achieves PSNR values between 45.92 dB and 48.33 dB at full embedding, with SSIM ranging from 0.9678 to 0.9805. These levels show that structural distortions are still well controlled, though slightly more pronounced than those seen in common images. However, when compared with Arham & Nugroho [5], which achieve PSNR values above 52 dB across most medical images, the proposed method exhibits lower visual fidelity, which can be attributed to its substantially larger payload. For example, on the MRI image, the proposed method achieves 45.92 dB, while Arham & Nugroho [5] produce 53.32 dB. Similarly, on Ultrasonography, the proposed method yields 47.81 dB, compared to 52.96 dB in [5]. As illustrated in Table 2 and Figs. 7 and 8, these results highlight the inherent trade-off between extremely high embedding capacity and visual quality. Higher payloads inevitably lead to increased distortion, while maintaining acceptable PSNR and SSIM levels.

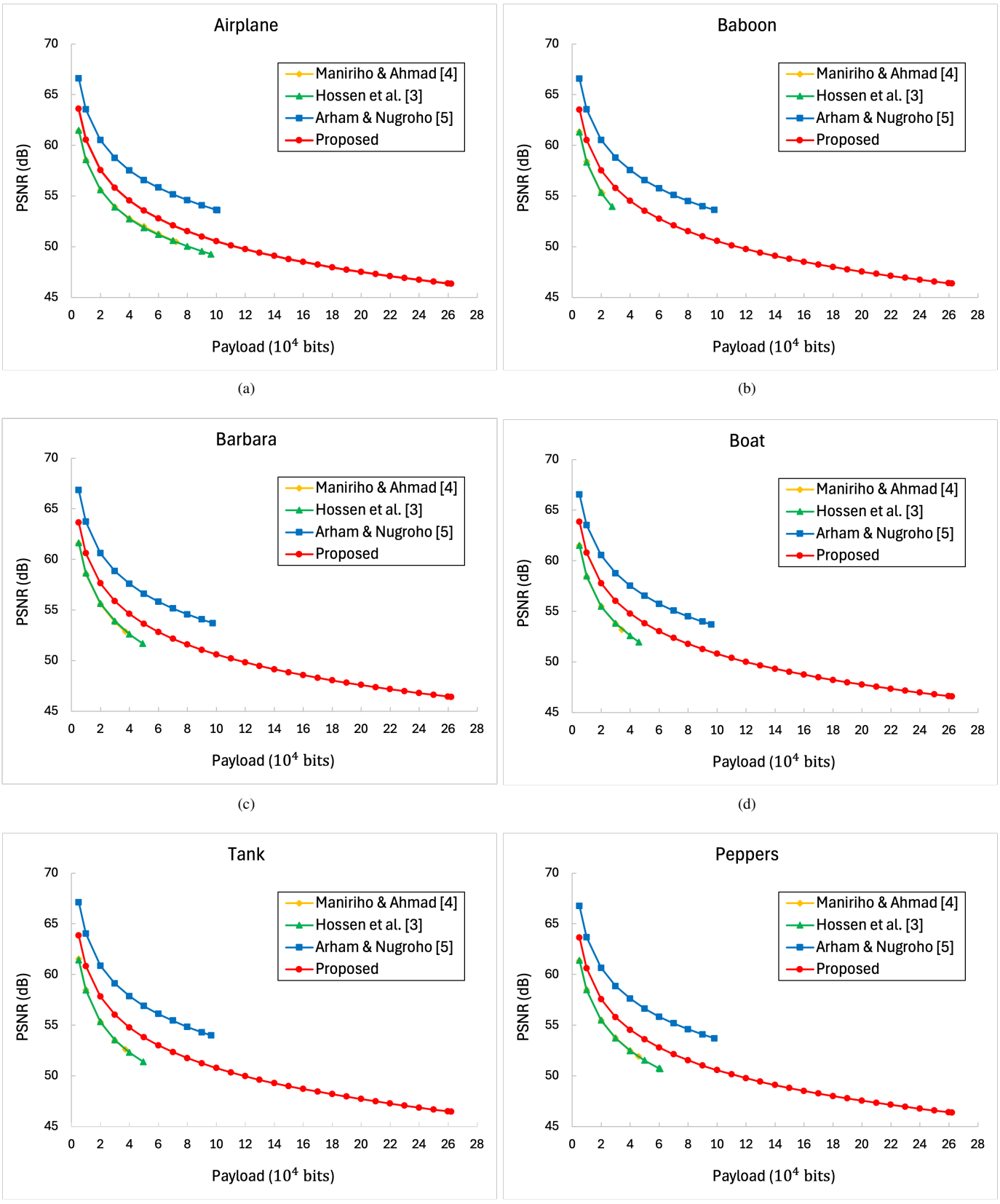

(a) (b)

(c) (d)

(e) (f)

Fig. 7. Comparison between the proposed method and previous works in terms of PSNR for different payload sizes on common images: (a) Airplane, (b) Baboon, (c) Barbara, (d) Boat, (e) Tank, and (f) Peppers.

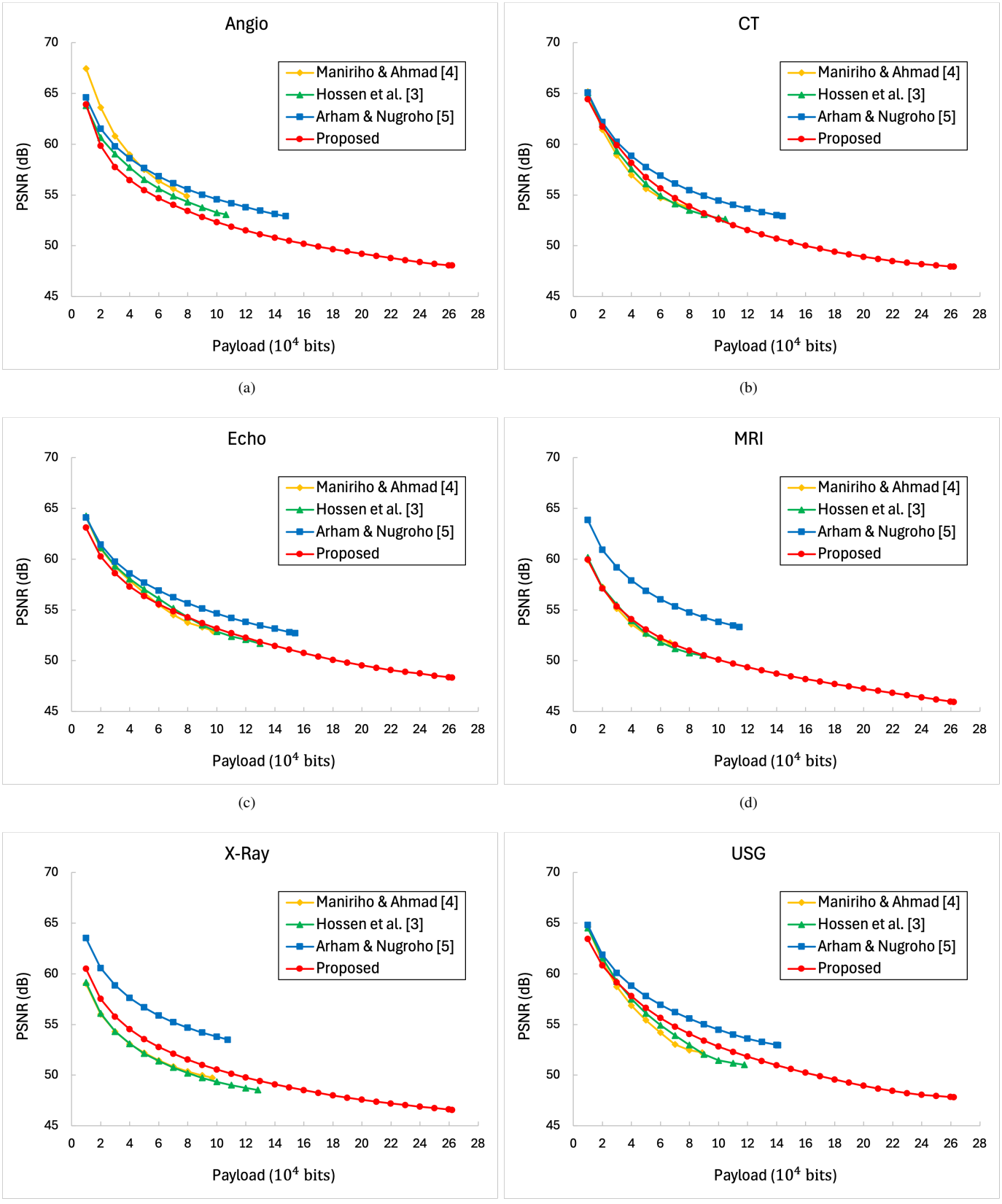

Fig. 8. Comparison of PSNR under various payload sizes on medical images using our method vs baselines: (a) Angiogram, (b) CT, (c) Echocardiogram, (d) MRI, (e) Radiograph, and (f) Ultrasonography.

To evaluate the statistical imperceptibility of the proposed watermarking scheme, we analyzed and compared the normalized histograms of the original (cover) images and their corresponding stego images. This comparison provides insight into the preservation of pixel-value distributions after watermark embedding and helps assess the method's robustness against histogram-based analysis. Figs. 9 and 10 illustrate the histogram distributions of the original and watermarked images for the common and medical image sets, respectively. The close similarity between the histograms before and after embedding indicates that the proposed method introduces minimal statistical distortion, supporting its imperceptibility and robustness against histogram-based detection.

For the common image set, the histogram patterns of the stego images closely resemble those of the original images. As shown in Table 3, the Euclidean and Chebyshev distances remain consistently small across all samples (below 0.02 and 0.006 in most cases). The correlation distance values are also low, indicating that the overall histogram structure is well preserved. Even for textured images such as Baboon and Barbara, the statistical deviations remain minimal. These results confirm that the proposed embedding process introduces negligible perturbation to pixel intensity distributions, making the scheme highly resilient to first-order histogram-based analysis.

Table 3. Difference in the histogram distribution for common images

Image	Euclidean	Chebyshev	Correlation
Airplane	0.0088	0.0042	0.0036
Baboon	0.0027	0.0006	0.0013
Barbara	0.0072	0.0020	0.0180
Boat	0.0149	0.0053	0.0197
Tank	0.1260	0.0358	0.6178
Peppers	0.0056	0.0032	0.0076
Average	0.0225	0.0069	0.0676

Table 4. Difference in the histogram distribution for medical images

Image	Euclidean	Chebyshev	Correlation
Angiogram	0.3488	0.2502	0.2850
CT	0.3226	0.2333	0.2698
Echocardiogram	0.3797	0.2738	0.2587
MRI	0.1709	0.1434	0.3270
Radiograph	0.0502	0.0366	0.1818
Ultrasonography	0.2975	0.2141	0.2697
Average	0.2667	0.1998	0.2859

In contrast, the medical image set shows relatively larger histogram deviations, as summarized in Table 4. The Euclidean distance ranges from 0.0502 to 0.3797, while the Chebyshev and Correlation distances also exhibit greater variability compared to common images. This behavior is expected due to the inherent characteristics of medical images, which typically contain narrow intensity ranges, high homogeneity, or pronounced histogram peaks (e.g., CT, angiogram, and echocardiogram images).

In such cases, even small modifications to pixel values may result in noticeable histogram shifts despite maintaining acceptable visual quality metrics. Nevertheless, the observed histogram variations in medical images do not affect the reversibility of the proposed scheme, as the original images are perfectly recovered after watermark extraction. The differences remain within acceptable statistical bounds and are consistent with the behavior reported in other reversible watermarking methods applied to diagnostic imaging. Overall, the analysis demonstrates that the proposed method ensures strong histogram consistency for common images and maintains statistically stable behavior for medical images, supporting its applicability for both general-purpose and medical imaging scenarios. It should be noted that histogram analysis provides a statistical perspective on intensity distribution changes and does not substitute for clinical or observer-based perceptual evaluation.

4.3. Performance Analysis

Computational efficiency is a key strength of the proposed method. As shown in Table 2, the proposed scheme requires only 0.61–0.66 seconds for embedding process on both common and medical images, which is significantly faster than existing approaches. In contrast, existing methods by Maniriho & Ahmad [4], Hossen et al. [3], and Arham & Nugroho [5] exhibit computational times in the range of 4.02–5.17 seconds, making them approximately 7–8 times slower. This performance improvement can be attributed to the simplicity of the bit-level expansion mechanism and the elimination of complex prediction, sorting, or multi-round optimization procedures. In terms of embedding rate (ER), the improvement is even more substantial. As summarized in Table 2, the proposed method achieves ER values of 395,390–426,944 bits/s, substantially exceeding competing techniques. The highest-performing baseline, Arham & Nugroho [5], reaches only 30,941–32,437 bits/s, while methods [3] and [4] remain below 24,000 bits/s. This translates to a throughput increase of more than 10× compared to the best prior technique and up to approximately 20× compared to prior methods.

Fig. 11 compares computational time of the proposed method with existing reversible watermarking techniques for both common and medical images. The proposed method consistently achieves the lowest execution time across all test cases, indicating that the simplicity of the bit-level expansion strategy contributes to improved computational efficiency and supports real-time or large-scale watermark embedding.

4.4. Embedding Map Analysis

To evaluate embedding map efficiency, we introduce a metric termed Embedding Map Efficiency (EME). EME is defined as the ratio between the embedding capacity and the size of the embedding map (Eq. 14). Here, C denotes the total number of watermark bits successfully embedded, while M represents the number of bits used to store the embedding map. A higher EME value indicates more efficient map usage.

$$EME = \frac{C}{M} \tag{14}$$

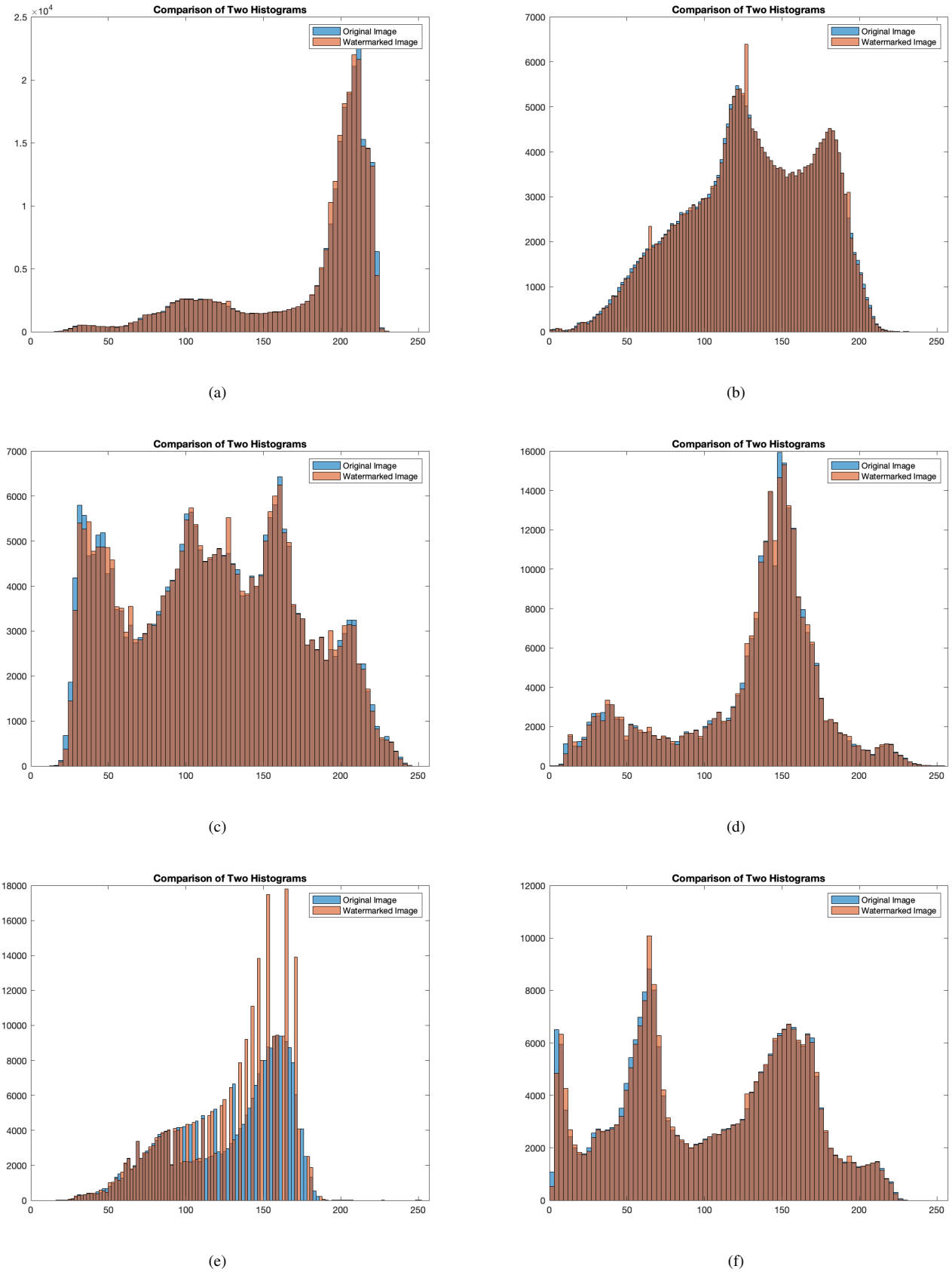

Fig. 9. Comparison of common image and stego image histograms: (a) Airplane, (b) Baboon, (c) Barbara, (d) Boat, (e) Tank, and (f) Peppers.

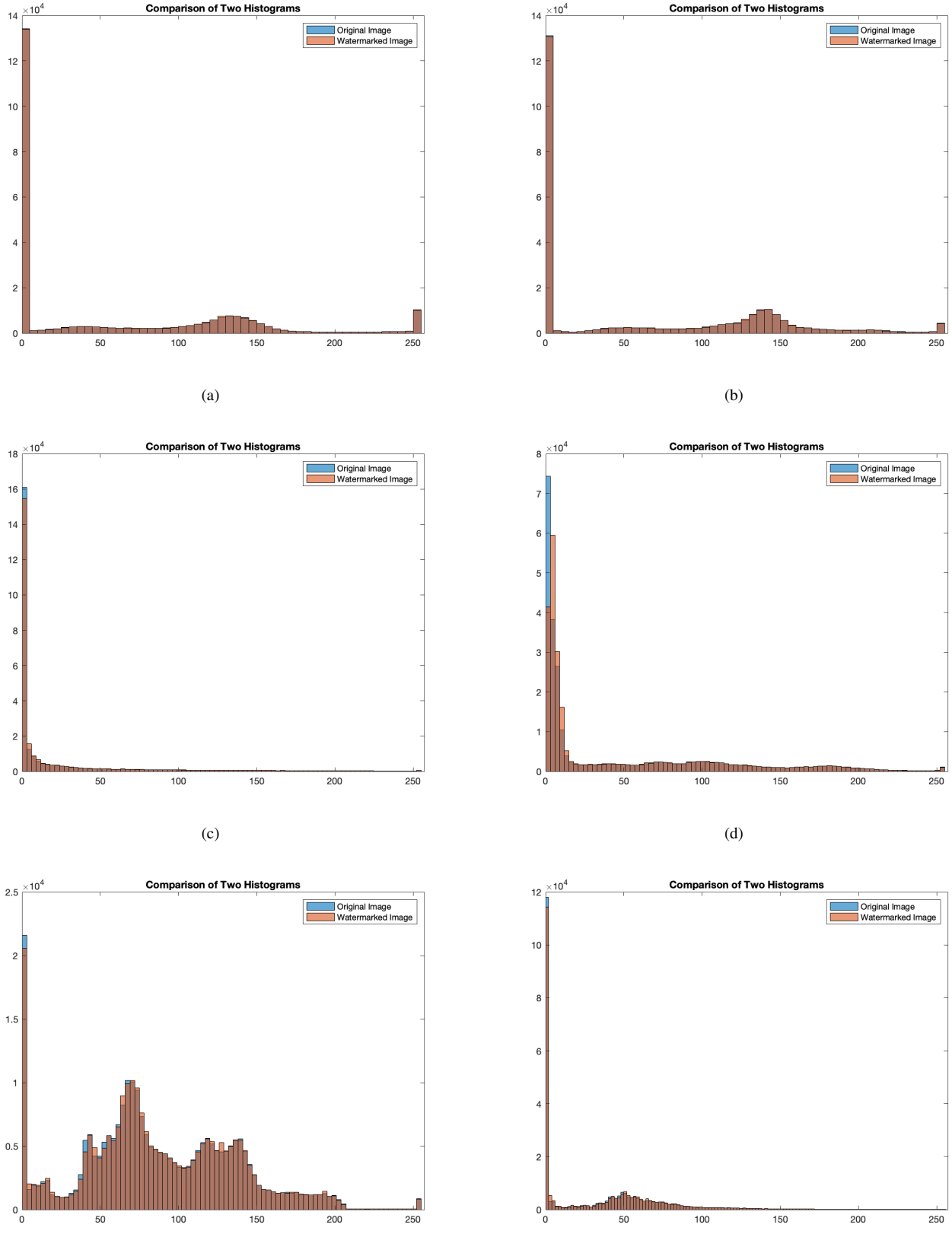

Fig. 10. Comparison of medical image and stego image histograms: (a) Angiogram, (b) CT, (c) Echocardiogram, (d) MRI, (e) Radiograph, and (f) Ultrasonography.

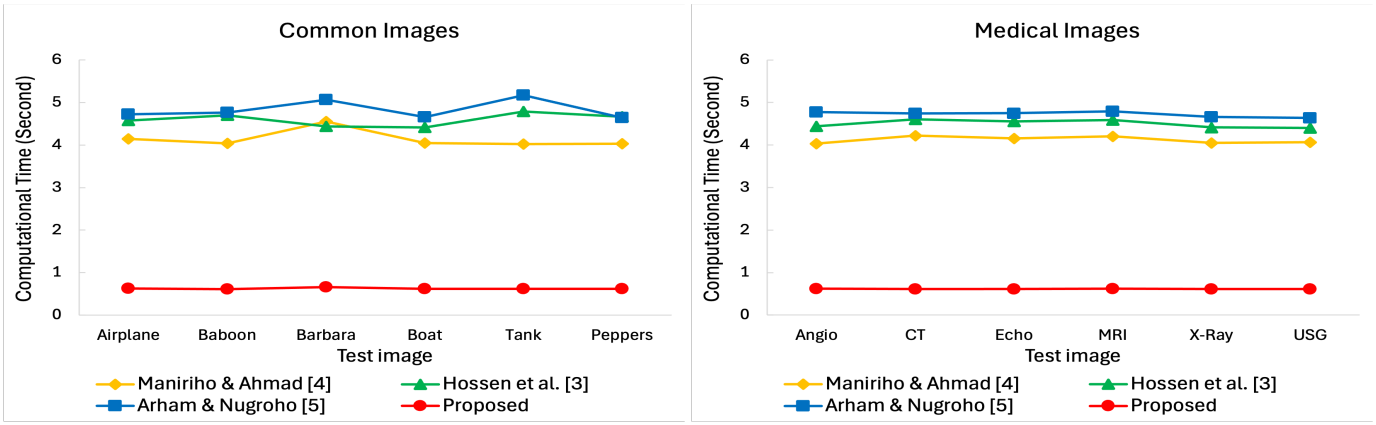

(a) (b)

Fig. 11. Comparison of computational time between the proposed method and existing methods for (a) common images and (b) medical images.

Here, C denotes the total number of watermark bits successfully embedded, while M represents the number of bits required to store the embedding map. A higher EME value indicates more efficient map usage.

For contextual comparison, it is important to consider the structural characteristics of the existing reversible watermarking methods. Maniriho and Ahmad [4] utilize 1×2 pixel blocks, requiring one map bit per block, leading to an embedding map size of approximately half the image, and supporting a maximum payload of 0.5 bits per pixel (bpp). Hossen et al.[3] employ 1×3 pixel blocks with 2 map bits per block, leading to an embedding map size of roughly two-thirds of the image and a maximum capacity of 0.66 bpp. Arham and Nugroho[5] further increase map overhead by using 2×2 blocks, requiring 3 map bits per block and achieving a maximum payload of 0.75 bpp.

In contrast, the proposed method assigns one map bit per pixel along with additional information required for pixel shifting. Although this design theoretically implies a larger map size, the adaptive expansion strategy enables embeddability for all pixels through controlled and reversible bit-level adjustments. As a result, the proposed method achieves a consistent embedding capacity of up to 1.0 bpp across all test images. Consequently, since $C = M$ for all cases, the proposed method attains indicating near-optimal map efficiency. Unlike block-based methods, whose effective capacity is constrained by non-expandable regions and map redundancy, the proposed approach fully utilizes the embedding map without introducing unused map entries. Therefore, the EME metric provides a clear measure of how effectively map overhead is converted into usable payload capacity without introducing unused map entries, while maintaining acceptable visual fidelity.

$$EME = \frac{C}{M} = 1.0,$$

As shown in Fig. 12, the proposed method achieves an Embedding Map Efficiency (EME) of 1.0 for both common and medical images, indicating that all embedding map bits are effectively translated into usable payload. For common images, the benchmark methods achieve average EME values of 0.3147 (Maniriho & Ahmad), 0.3140 (Hossen et al.), and 0.4978 (Arham & Nugroho), whereas the proposed method consistently attains a maximum EME value of 1.0. This result confirms that, unlike block-based schemes, the proposed pixel-level expansion strategy effectively reduces map redundancy and maximizes embedding efficiency.

A similar trend is observed for medical images, where the proposed method maintains EME= 1.0 across all six cases. In contrast, existing methods achieve average efficiencies of 0.6446, 0.6447, and 0.6858, respectively. The ability to maintain consistent maximum efficiency across different image types with varying texture and structural complexity highlights the robustness and adaptability under the evaluated conditions. Overall, the results confirm that the proposed method not only maximizes embedding capacity but also optimizes embedding map usage. By ensuring that every pixel contributes to reversible expansion, the proposed approach achieves perfect embedding map efficiency, outperforming existing block-based techniques whose efficiency is inherently constrained by their structural design.

4.5. *Comprehensive Comparison*

The experimental results clearly illustrate an inherent trade-off between embedding capacity, visual quality, and reversibility. By enforcing full bit-level expansion on every pixel, the proposed method achieves the theoretical maximum capacity of 1.0 bpp, which inevitably results in increased pixel modifications compared to existing methods that embed only in selectively expandable regions. This design choice explains the observed reduction in PSNR relative to baseline schemes, particularly at full payload. However, the reversibility of the proposed method is ensured by the shifting map mechanism, enabling perfect recovery of the original image without any loss. Moreover, despite lower PSNR values, the obtained SSIM scores remain consistently high, indicating that structural distortions are well controlled. When combined with the substantial gains in embedding rate, computational efficiency, and embedding map efficiency, the results demonstrate that the proposed scheme offers a well-balanced and practically meaningful trade-off for high-capacity reversible watermarking applications, especially in medical imaging scenarios.

Table 2 and Figs. 6–12 provide a comprehensive summary of all evaluation metrics obtained in this study. Overall, the

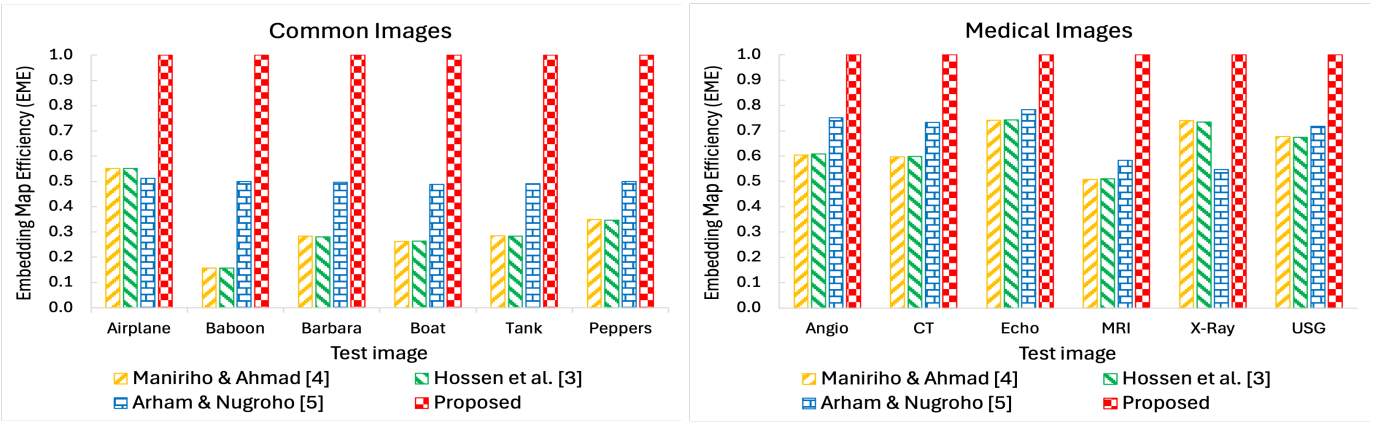

(a) (b)

Fig. 12. Comparison of Embedding Map Efficiency (EME) between the proposed method and existing methods for (a) common images and (b) medical images.

proposed reversible watermarking scheme consistently demonstrates superior performance across most evaluated metrics.

- **Embedding Capacity:** The proposed method approaches the theoretical maximum payload of 1.0 bpp (262,144 bits for a 512×512 image), which is substantially higher than Maniriho & Ahmad [4] (0.5 bpp), Hossen et al. [3] (0.66 bpp), and Arham & Nugroho [5] (0.75 bpp). This improvement is clearly reflected in Table 2.

- **Embedding Capacity:** The proposed method achieves the theoretical maximum payload of 1.0 bpp (262,144 bits for a 512×512 image), which is significantly higher than Maniriho & Ahmad [4] (0.5 bpp), Hossen et al. [3] (0.66 bpp), and Arham & Nugroho [5] (0.75 bpp). This improvement is reflected in Table 2. It should be noted that achieving this maximum capacity inherently involves a trade-off between embedding payload and visual quality; however, the proposed bit-level adaptive expansion strategy mitigates this trade-off through controlled and reversible pixel modifications.

- **Visual Quality:** Despite embedding the largest payload, the proposed method maintains acceptable to high visual fidelity, yielding PSNR values generally above 46 dB and SSIM above 0.97. As shown in Figs. 6 and 7, the proposed scheme better preserves structural details under high payload conditions than existing methods, particularly for common images. It is important to note that PSNR values reported in the literature are often achieved at payloads below 0.5 bpp, whereas the proposed method evaluates visual quality under the challenging condition of 1.0 bpp. For medical images, the reversible nature of the proposed scheme ensures that the original image can be fully recovered after watermark extraction, thereby preserving diagnostic integrity.

- **Computational Time:** The proposed method requires only 0.67–0.73 seconds per image, which is approximately 5–7 times faster than competing approaches that require between 4.1 and 5.2 seconds (see Fig. 11).

- **Embedding Rate:** With an embedding throughput exceeding 380,000 bits/s for all test cases, the proposed scheme achieves a rate more than 10 times higher than Arham & Nugroho [5], whose throughput peaks around 32,000 bits/s. This highlights its suitability for real-time or high-throughput applications.

- **Embedding Map Efficiency (EME):** As shown in Fig. 12, the proposed method achieves an EME of 1.0 for every common and medical image. This means the entire embedding map is fully utilized, and with no redundant map entries under the proposed design. In contrast, existing methods yield significantly lower EME values, with averages of 0.3147 (Maniriho & Ahmad), 0.3140 (Hossen et al.), and 0.4978 (Arham & Nugroho) for common images, and 0.6446, 0.6447, and 0.6858 for medical images, respectively.

Overall, the experimental results demonstrate that the proposed scheme achieves a favorable balance of capacity, visual quality, computational efficiency, and embedding map utilization. These characteristics make it particularly suitable for applications such as medical imaging, where embedding large volumes of patient data or diagnostic information is required without compromising clinical usability.

5. Conclusion

This paper presents a novel high-capacity reversible watermarking scheme that integrates an adaptive bit-level expansion mechanism with pixel-class-driven shifting. The proposed method addresses the key trade-offs involved in reversible data hiding namely capacity, visual quality, reversibility, and computational efficiency by classifying pixels into expandable and non-expandable sets and adaptively transforming them to maximize embedding feasibility. The technique embeds data directly into the 2-bit LSB of each pixel while maintaining full image reversibility. By defining two-pixel sets (P_0, and P_1), and rigorously proving that bounded shifts can transform non-expandable pixels into expandable ones, the method ensures predictable inverse shifting behavior and exact restoration of the original image. Extensive experiments on both common and medical

image datasets demonstrate that the proposed scheme significantly outperforms existing state-of-the-art methods. It consistently achieves an embedding capacity of 1.0 bpp across all tested images representing a 2.5-3.0× improvement over prior approaches, while achieving 5-7× faster embedding time and up to 10× higher throughput. Despite the increased payload, the watermarked images maintain high visual fidelity, with PSNR values above 46.9 dB and SSIM above 0.97, making the method well suited for real-time and medical imaging workflows. Overall, the proposed framework provides a scalable and computationally efficient framework with full reversibility for high-capacity data embedding. It offers practical value in applications requiring strict integrity preservation, such as medical image security, legal forensics, and authenticated data exchange. Future work will investigate extensions to color images, multi-layer watermarking, and integration with lightweight cryptographic primitives to further enhance security and privacy.

Acknowledgment

This work was supported by the Indonesia Endowment Fund for Education (LPDP), Ministry of Finance, Republic of Indonesia. The authors also acknowledge the use of AI-based language tools for improving the clarity and coherence of the manuscript.

References

1. A. Arham, H. A. Nugroho, *Block-based optimization for enhancing reversible watermarking using reduce difference expansion*, Commun. Sci. Technol. 9 (2024) 57-64.
2. J. Tian, *Reversible data embedding using a difference expansion*, IEEE Trans. Circuits Syst. Video Technol. 13 (2003) 890-896.
3. M. S. Hossen, T. Ahmad, N. J. De La Croix, *Data hiding scheme using difference expansion and modulus function*, 2023 2nd Int. Conf. Innov. Technol. (INOCON), IEEE, 2023, pp. 1-6.
4. P. Maniriho, T. Ahmad, *Information hiding scheme for digital images using difference expansion and modulus function*, J. King Saud Univ. Comput. Inf. Sci. 31 (2019) 335-347.
5. A. Arham, H. A. Nugroho, *Enhanced reversible data hiding using difference expansion and modulus function with selective bit blocks in images*, Cybersecur. 7 (2024) 61.
6. F. Li, L. Zhang, C. Qin, K. Wu, *Reversible data hiding for JPEG images with minimum additive distortion*, Inf. Sci. 595 (2022) 142-158.
7. F. Wu, J. Sun, S. Zhang, N. Xiong, H. Zhong, *Efficient reversible data hiding via two layers of double-peak embedding*, Inf. Sci. 644 (2023) 119264.
8. A. Arham, H. A. Nugroho, T. B. Adji, *Multiple layer data hiding scheme based on difference expansion of quad*, Signal Process. 137 (2017) 52-62.
9. M. H. A. Al Huti, T. Ahmad, S. Djanali, *Increasing the capacity of the secret data using depixels blocks and adjusted RDE-based on grayscale images*, Int. Conf. Inf. Commun. Technol. Syst. (ICTS), IEEE, 2015, pp. 225-230.
10. Z. Syahlan, T. Ahmad, *Reversible data hiding method by extending reduced difference expansion*, Int. J. Adv. Intell. Inform. 5 (2019) 101-112.
11. S. M. Abdullah, A. A. Manaf, *Multiple layer reversible images watermarking using enhancement of difference expansion techniques*, Int. Conf. Netw. Digit. Technol., Springer, 2010, pp. 333-342.
12. Z. Zhang, M. Zhang, L. Wang, *Reversible image watermarking algorithm based on quadratic difference expansion*, Math. Probl. Eng. 2020 (2020) 1806024.
13. T.-S. Nguyen, V.-T. Huynh, P.-H. Vo, *A novel reversible data hiding algorithm based on enhanced reduced difference expansion*, Symmetry. 14 (2022) 1726.
14. B. Ou, Y. Zhao, *High capacity reversible data hiding based on multiple histograms modification*, IEEE Trans. Circuits Syst. Video Technol. 30 (2019) 2329-2342.
15. W. Qi, X. Li, T. Zhang, Z. Guo, *Optimal reversible data hiding scheme based on multiple histograms modification*, IEEE Trans. Circuits Syst. Video Technol. 30 (2019) 2300-2312.
16. W. He, G. Xiong, Y. Wang, *Reversible data hiding based on adaptive multiple histograms modification*, IEEE Trans. Inf. Forensics Secur. 16 (2021) 3000-3012.
17. H. Wu, X. Li, X. Luo, X. Zhang, Y. Zhao, *General expansion-shifting model for reversible data hiding: Theoretical investigation and practical algorithm design*, IEEE Trans. Circuits Syst. Video Technol. 32 (2022) 5989-6001.
18. W. He, Z. Cai, Y. Wang, *High-fidelity reversible image watermarking based on effective prediction error-pairs modification*, IEEE Trans. Multimedia. 23 (2020) 52-63.
19. W. He, Z. Cai, *Reversible data hiding based on dual pairwise prediction error expansion*, IEEE Trans. Image Process. 30 (2021) 5045-5055.
20. Q. Chang, X. Li, Y. Zhao, R. Ni, *Adaptive pairwise prediction-error expansion and multiple histograms modification for reversible data hiding*, IEEE Trans. Circuits Syst. Video Technol. 31 (2021) 4850-4863.
21. F. Aziz, T. Ahmad, A. H. Malik, M. I. Uddin, S. Ahmad, M. Sharaf, *Reversible data hiding techniques with high message embedding capacity in images*, PLoS One. 15 (2020) e0231602.
22. X. Wang, X. Wang, B. Ma, Q. Li, Y.-Q. Shi, *High precision error prediction algorithm based on ridge regression predictor for reversible data hiding*, IEEE Signal Process. Lett. 28 (2021) 1125-1129.
23. W. He, Z. Cai, *An insight into pixel value ordering prediction-based prediction-error expansion*, IEEE Trans. Inf. Forensics Secur. 15 (2020) 3859-3871.
24. A. Roy, R. S. Chakraborty, *Toward optimal prediction error expansion-based reversible image watermarking*, IEEE Trans. Circuits Syst. Video Technol. 30 (2019) 2377-2390.
25. P.-H. Kim, K.-W. Ryu, K.-H. Jung, *Reversible data hiding scheme based on pixel-value differencing in dual images*, Int. J. Distrib. Sens. Netw. 16 (2020) 1550147720911006.
26. T. Zhang, X. Li, W. Qi, Z. Guo, *Location-based PVO and adaptive pairwise modification for efficient reversible data hiding*, IEEE Trans. Inf. Forensics Secur. 15 (2020) 2306-2319.
27. M. Fan, S. Zhong, X. Xiong, *Reversible data hiding method for interpolated images based on modulo operation and prediction-error expansion*, IEEE Access. 11 (2023) 27290-27302.
28. A. Mohammadi, M. Nakhkash, M. A. Akhaee, *A high-capacity reversible data hiding in encrypted images employing local difference predictor*, IEEE Trans. Circuits Syst. Video Technol. 30 (2020) 2366-2376.
29. Y. Wang, Z. Cai, W. He, *High capacity reversible data hiding in encrypted image based on intra-block lossless compression*, IEEE Trans. Multimedia. 23 (2020) 1466-1473.
30. Y. Wang, W. He, *High capacity reversible data hiding in encrypted image based on adaptive MSB prediction*, IEEE Trans. Multimedia. 24 (2021) 1288-1298.
31. K.-M. Chen, *High capacity reversible data hiding based on the compression of pixel differences*, Mathematics. 8 (2020) 1435.
32. P. Puteaux, W. Puech, *A recursive reversible data hiding in encrypted images method with a very high payload*, IEEE Trans. Multimedia. 23 (2020) 636-650.
33. C. Yu, X. Zhang, X. Zhang, G. Li, Z. Tang, *Reversible data hiding with hierarchical embedding for encrypted images*, IEEE Trans. Circuits Syst. Video Technol. 32 (2021) 451-466.
34. USC-SIPI, *Image database*, 2025. Available: https://sipi.usc.edu/database/database.php.
35. Partners Infectious Disease Images, *eMicrobes digital library*, 2025. Available: http://www.idimages.org.